International Journal of
Molecular Sciences

MDPI

Article

A New Ursane-Type Pentacyclic Triterpenoid from the Tree Bark of *Sandoricum koetjape*: Antibacterial, DFT, and Molecular Docking Study

Husnul Khatimah [1], Elvira Hermawati [1,*], Fadjar Mulya [2], Muhammad Ikhlas Abdjan [3], Thanawit Kuamit [4] and Ade Danova [1,*]

[1] Organic Chemistry Division, Department of Chemistry, Faculty of Mathematics and Natural Sciences, Institut Teknologi Bandung, Jl. Ganesha No.10, Bandung 40132, Indonesia; husnulkhatimah52@gmail.com
[2] Nanotechnology Engineering Program, Faculty of Advanced Technology and Multidiscipline, Universitas Airlangga, Surabaya 60115, Indonesia; fadjar.mulya@ftmm.unair.ac.id
[3] Department of Chemistry, Faculty of Mathematics and Natural Sciences, Universitas Negeri Surabaya, Surabaya 60213, Indonesia; muhammadabdjan@unesa.ac.id
[4] Center of Excellence in Computational Chemistry (CECC), Department of Chemistry, Faculty of Science, Chulalongkorn University, Bangkok 10330, Thailand; thanawit.kuamit@chula.ac.th
* Correspondence: elvira.hermawati@itb.ac.id (E.H.); adedanova@itb.ac.id (A.D.)

Abstract

Natural products have played an important role in the discovery and development of antibacterial agents. This paper described the isolation of a new ursane-type pentacyclic triterpenoid, (18β,19αH)-3-oxo-urs-12-en-27α-oic acid (**2**), from the tree bark of *Sandoricum koetjape* Merr. Along with this, five known compounds—β-caryophyllene oxide (**1**), bryononic acid (**3**), 7-deacetylgedunin (**4**), 7-deacetyl-7-oxogedunin (**5**), and 12,20-dihydroxydammar-24-en-3-one (**6**)—were successfully isolated, and one compound, 12β-hydroxydammarenolic acid (**7**), was reported in our previous report. All compounds (**1**–**7**) were tested with their antibacterial properties against two Gram-positive (*Enterococcus faecalis* and *Staphylococcus saprophyticus*) and two Gram-negative (*Citrobacter freundii* and *Salmonella enterica*) bacteria. The structures of the isolated compounds were elucidated using NMR spectroscopy and mass spectrometry data. A preliminary antibacterial assay showed that only compound **7** inhibited the growth of the tested bacteria, with an inhibition zone diameter of 7.5–9 mm at a concentration of 1 mg/mL. DFT analyses explained electronic profiles with HOMO-LUMO gaps (4.54–6.34 eV) and electrophilicity from 1.73 to 4.39 eV. To elucidate the antibacterial mechanism of compound **7**, a molecular docking study was conducted. The findings from both in vitro and in silico analyses suggest that compound **7** is a promising antibacterial candidate for further investigation.

Keywords: antibacterial; density functional calculation; docking study; *Sandoricum koetjape*; terpenoids

check for updates

Received: 26 September 2025
Revised: 18 October 2025
Accepted: 23 October 2025
Published: 25 October 2025

Citation: Khatimah, H.; Hermawati, E.; Mulya, F.; Abdjan, M.I.; Kuamit, T.; Danova, A. A New Ursane-Type Pentacyclic Triterpenoid from the Tree Bark of *Sandoricum koetjape*: Antibacterial, DFT, and Molecular Docking Study. *Int. J. Mol. Sci.* **2025**, *26*, 10389. https://doi.org/10.3390/ijms262110389

Copyright: © 2025 by the authors. Licensee MDPI, Basel, Switzerland. This article is an open access article distributed under the terms and conditions of the Creative Commons Attribution (CC BY) license (https://creativecommons.org/licenses/by/4.0/).

1. Introduction

Since the discovery of penicillin in 1928, antibiotics have been crucial for public health, saving the lives of millions of people worldwide. However, in recent years, it has been discovered that an increasing number of bacteria are developing resistance [1]. Antibacterial resistance is a global public health challenge that is thought to have contributed to 4.95 million deaths in 2019, primarily in low- and middle-income countries [2]. Antibiotic resistance has been reported in bacteria that cause common diseases such as urinary tract

infections, pneumonia, bloodstream infections, skin infections, etc. [3]. In 2024, the World Health Organization (WHO) published a list of antibiotic-resistant priority pathogens, which pose a significant threat to people, and therefore new treatments are urgently needed. Gram-negative bacteria that are resistant to last-resort antibiotics, like *Acinetobacter baumannii* and various *Enterobacter pathogens*, as well as *Mycobacterium tuberculosis*, are classified as critical priority due to their ability to transfer resistance genes. Other bacteria, including *Salmonella*, *Shigella*, *Pseudomonas aeruginosa*, *Staphylococcus aureus*, *Neisseria gonorrhoeae*, and *Enterococcus faecium*, are categorized as a high priority because of their resistance to existing treatments and the significant burden of infection associated with these pathogens [2].

Natural products have played a crucial role in the discovery and development of antibacterial agents as they continue to provide new chemical structures [4]. For almost four decades, from 1981 to 2019, around 48% of approved antibacterial agents were derived from natural products and derivatives [5]. Terpenes and their derivatives have been studied and found to have significant antimicrobial activities, demonstrating bacteriostatic and bactericidal effects against tested pathogens through various mechanisms of action [6]. Pentacyclic triterpenoids, including oleanolic and ursolic acids, isolated from *Alstonia scholaris* showed significant antibacterial activity against Gram-positive bacteria, *E. faecalis*, *L. monocytogenes*, and *B. cereus* [7]. Recently, a series of semisynthetic triterpenoids with A-ring azepano- and A-seco-fragment substituents at C3 and C28 demonstrated a strong bacteriostatic effect against Methicillin-resistant *S. aureus* (MIC $\leq$ 0.15 μM), exceeding the clinically used antibiotic vancomycin (MIC = 0.625 μM) [8]. Moreover, an oleanane derivative also showed significant antimicrobial activity against both Gram-positive and Gram-negative bacteria [9].

Sandoricum koetjape Merr., a species of Meliaceae, has some potential secondary metabolites. Traditionally, plants have been used to address digestive issues and inflammatory diseases [10]. Phytochemical studies of the leaves, seeds, fruit hulls, stem barks, and barks of *S. koetjape* have revealed the presence of terpenoids, predominantly pentacyclic triterpenoids and limonoids [11–22]. Pentacyclic triterpenoids were dominated by oleanane- and multiflorane-type triterpenes, while the limonoids were dominated by andirobin and trijugin types. Some of these compounds have been shown to be effective antifeedants [20] and anti-inflammatory agents [18], and to exhibit potential cytotoxicity against several cancer cells [11,12,14,21]. Recently, a tirucallane-type tetracyclic triterpene isolated from the seed and fruit peels of *S. koetjape* exhibited weak activity against InsR [13]. Additionally, two new cycloartane-type tetracyclic triterpenes isolated from the leaves also showed promising α-glucosidase inhibitory activity [23]. To date, the isolation of secondary metabolites from the tree bark of *S. koetjape* remains limited. Previously, we reported the isolation of a new seco-dammarane triterpene, 12β-hydroxydammarenolic acid (**7**), and its inhibitory properties against several receptor tyrosine kinases [24]. In searching for antibacterial agents from natural products, in this study, we report our isolation, structural elucidation, and preliminary biological evaluation against four bacteria of a new pentacyclic triterpenoid (**2**) and five known compounds: limonoids (**4**, **5**), triterpenoids (**3**, **6**), and sesquiterpenoid (**1**) from the tree bark of MeOH extract of *S. koetjape* from Pandeglang, Banten, Indonesia. Furthermore, Density Functional Theory (DFT) calculations were performed to study the reactivity and stability of all compounds (**1**–**7**), and molecular docking analysis was conducted to study the molecular interaction between a potent compound (**7**) and PTP1B as the targeted protein.

2. Results

2.1. Identification of Isolated Compounds from S. koetjape

The tree bark powders of *S. koetjape* were dried and extracted with MeOH, then fractionated and purified using chromatographic techniques to obtain β-caryophyllene oxide (**1**), (18β,19αH)-3-oxo-urs-12-en-27α-oic acid (**2**), bryononic acid (**3**), 7-deacetylgedunin (**4**), 7-deacetyl-7-oxogedunin (**5**), 12,20-dihydroxydammar-24-en-3-one (**6**), and 12β-hydroxydammarenolic acid (**7**) (Figure 1), which have been reported against eight receptor tyrosine kinases [24]. Two gedunin-type limonoids (**4**, **5**) were first isolated from *S. koetjape*, although these compounds have been isolated from other Meliaceae species [25,26]. The dammarane-type triterpenes (**6**, **7**) [24] were also isolated from this plant for the first time, whereas tetracyclic triterpenoids have rarely been found in this plant. Moreover, this is the first report of the occurrence of **2** as a new ursane-type pentacyclic triterpene.

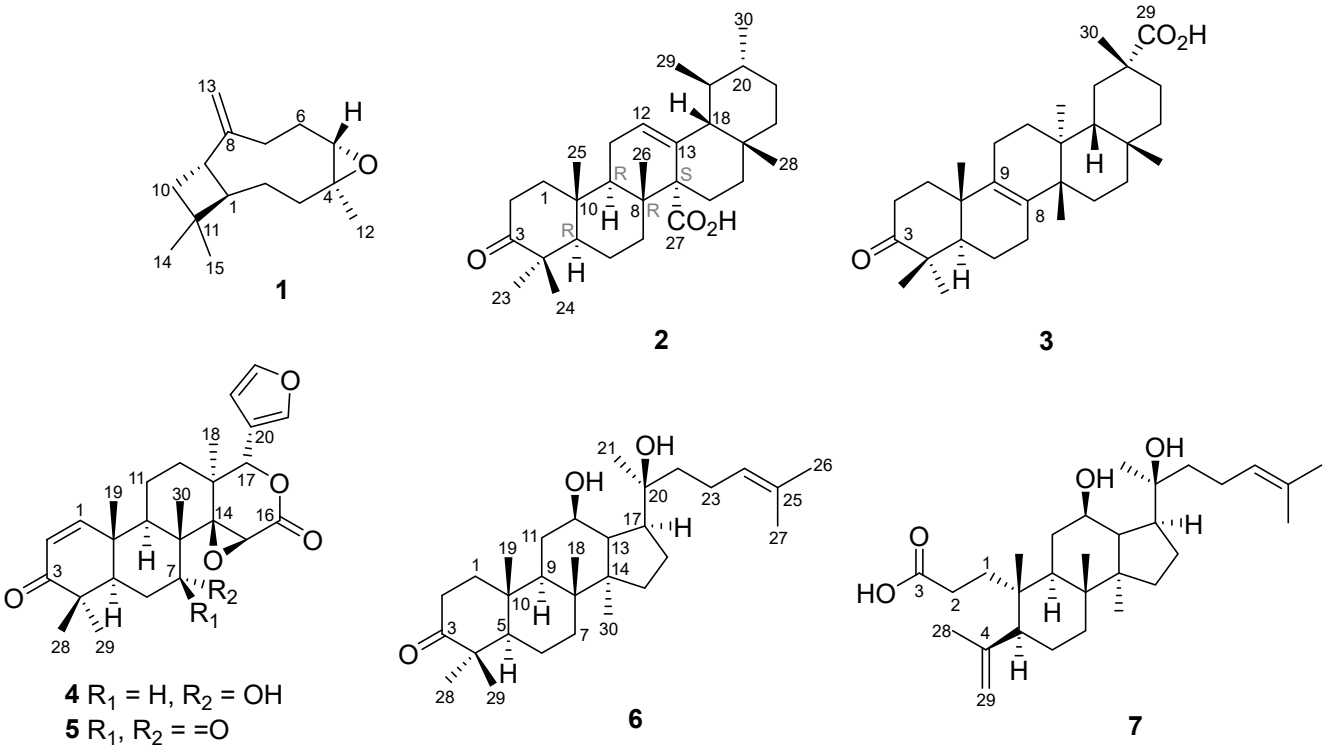


Figure 1. Structures of isolated compounds **1**–**7**.

Compound **2** was obtained as an optically active ($[\alpha]^{23}_{D}$ +142.0, c 0.1; $CHCl_3$) white powder. HRESIMS analysis revealed its molecular formula as $C_{30}H_{46}O_3$, with a molecular ion peak $[M-H]^-$ at *m*/*z* 453.3367 (calcd. 453.3369). The ^{13}C-NMR spectrum (Table 1; Figure S8) showed 30 carbon signals, including a trisubstituted alkene (δ_C 128.4 and 133.2), a carboxylic group (δ_C 180.9), a ketonic carbonyl (δ_C 217.9), a pair of vicinal methyls (δ_C 17.8 and 21.4), five quaternary sp^3 carbons (δ_C 47.1; 39.8; 36.6; 55.8; 33.7), and five additional methyl groups (δ_C 27.0; 21.3; 16.4; 18.1; 29.0). These functionalities represent three of the eight degrees of unsaturation, suggesting that **2** has a pentacyclic skeleton. The ^{1}H-NMR spectrum (Table 2; Figures S6 and S7) exhibited five singlet methyl signals (δ_H 1.06; 1.03; 1.05; 1.07; 0.84), one doublet methyl (δ_H 0.79), a broad singlet methyl (δ_H 0.86) in the upfield region, and an olefinic proton (δ_H 5.58) in the downfield region, which are typical for ursane-type triterpene [27,28]. The ketonic carbonyl was assigned to C-3 based on the HMBC correlations of H-1, H-2, and the pair of gem-dimethyl protons (H-23 and H-24) with the carbonyl group. The HMBC correlation between δ_H 1.77 (H-15β), δ_H 1.98 (H-15α), and δ_C 180.9 (C-27) indicated that the carboxylic acid group was attached to C-14. Furthermore,

the absence of methyl proton correlation with the olefinic carbon also supported that C-27 was oxidized to the carboxylic acid group (Figure 2). The relative stereochemistry was further elucidated based on proton coupling constants and NOE correlations observed in the ROESY spectrum (Figure S11, Table S1). The α-axial orientation of H-9 was deduced from its coupling constant (J = 11.0 and 5.45 Hz). The larger J value corresponds to trans-diaxial coupling, whereas the smaller one indicates an axial-equatorial interaction with H-11, thereby confirming the axial orientation of H-9. The cross-peaks between H-5/H-9, H-5/H-23, and H-9/H-11α indicated that they were on the same face in the α-configuration. In addition, the axial orientation of H-15β (δ_H 1.77) was inferred from the contour pattern. NOE correlations between H-15β/H-26, H-15β/H-28, H-28/H-18, and H-18/H-20 suggested that they were on the β-configuration. Furthermore, the methine proton at δ_H 2.11 (td, J = 13.62; 3.85 Hz, H-16) indicated an α-axial orientation. This proton showed a NOESY correlation with H-19, suggesting that H-19 is also in the α-configuration, whereas C-29 is β-oriented. This assignment was further supported by the observed NOESY correlation between H-29 and H-12 olefinic proton. Detailed analysis of 1D and 2D NMR spectra indicated that compound **2** possessed a skeleton similar to that of (14*S*)-3-oxo-18α,19αH-urs-12-en-27α-oic acid [29], differing in the β-axial orientation of H-18 (Figure 2). The absolute configurations at C-5, C-8, C-9, and C-14 were determined to be 5*R*, 8*R*, 9*R*, and 14*S*, respectively, based on a comparison with previously reported ursane-type triterpenoids [30], which is consistent with the stereochemistry of the α-amyrin-derived ursane skeleton. Thus, compound **2** was assigned as (18β,19αH)-3-oxo-urs-12-en-27α-oic acid. To the best of our knowledge, this is the first report of an ursane-type pentacyclic triterpenoid isolated from *S. koetjape*. Moreover, the oxygenation at C-27 is also rarely found in this plant.

Table 1. ^{13}C-NMR data of compounds **2**–**6** in $CDCl_3$.

Position	2	3	4	5	6
1	39.3	35.4	157.8	155.9	39.8
2	34.0	34.4	125.8	126.4	34.1
3	217.9	218.2	205.6	203.2	217.8
4	47.1	47.1	44.2	45.2	47.4
5	54.6	51.2	44.6	54.6	55.3
6	19.7	20.6	27.3	36.7	19.7
7	36.0	34.2	69.7	208.2	34.1
8	39.8	134.9	43.7	53.4	51.6
9	45.9	132.7	38.0	47.6	49.4
10	36.6	30.9	40.2	39.6	36.8
11	22.9	20.5	15.1	17.2	31.5
12	128.4	30.0	26.4	32.2	70.7
13	133.2	37.1	38.4	37.7	48.0
14	55.8	42.2	70.1	65.6	39.7
15	22.4	25.2	57.8	53.6	31.0
16	28.9	27.7	168.3	166.9	26.5
17	33.7	37.5	78.5	78.0	53.4
18	60.3	44.5	17.8	20.9	15.4
19	37.7	29.5	19.9	19.8	15.9

Table 1. *Cont.*

Position	2	3	4	5	6
20	39.6	40.4	120.6	120.2	74.7
21	30.4	30.5	141.2	141.0	27.1
22	40.8	36.8	110.0	109.8	34.3
23	27.0	21.1	143.0	143.1	22.4
24	21.3	26.8	-	-	124.8
25	16.4	19.5	-	-	132.0
26	18.1	21.7	-	-	25.8
27	180.9	18.1	-	-	17.8
28	29.0	31.1	27.3	27.0	21.0
29	17.8	185.1	21.5	20.6	26.7
30	21.4	32.7	18.7	17.4	16.8

Table 2. ^{1}H-NMR data of compounds **2**–**6** in $CDCl_3$.

Position	2	3	4	5	6
1	1.57 (*m*); 1.93 (*m*)	2.02 (*m*); 1.53 (*m*)	7.10 (*d*, 10.2)	7.11 (*d*, 10.2)	1.47 (*m*)
2	2.46 (*m*)	2.45 (*m*); 2.53(*m*)	5.84 (*d*, 10.2)	5.92 (*d*, 10.2)	2.44 (*m*); 2.51 (*m*)
5	1.35 (*m*)	1.61 (*m*)	2.48 (*m*)	2.18 (*m*)	1.36 (*m*)
6	1.43 (*m*)	1.95 (*m*)	1.66 (*m*); 1.90 (*m*)	2.41 (*dd*, 2.9; 13.9); 2.93 (*t*, 14.2)	1.52 (*m*)
7	1.16 (*m*); 1.75 (*m*)	2.03 (*m*); 0.89 (*m*)	3.57 (*s*)	-	1.34 (*m*); 1.55 (*m*)
9	2.33 (*dd*, 5.45; 11.0)	-	2.52 (*m*)	2.21 (*m*)	1.51 (*m*)
11	2.01 (*m*)	1.62 (*m*); 1.44 (*m*)	1.80 (*m*); 1.97 (*m*)	1.80 (*m*); 2.00 (*m*)	1.31 (*m*); 1.85 (*m*)
12	5.58 (*qui*, 2.4)	1.67 (*m*); 1.28 (*m*)	1.54 (*m*); 1.71 (*m*)	1.48 (*dt*, 12.43; 8.84); 1.86 (*m*)	3.60 (*td*, 10.41; 5.08)
13	-	-	-	-	1.76 (*t*, 10.65)
15	1.77 (*m*); 1.98 (*m*)	1.46 (*m*); 1.31 (*m*)	3.91 (*s*)	3.87 (*s*)	1.05 (*m*); 1.51 (*m*)
16	0.91 (*m*); 2.11 (*td*, 13.62; 3.85)	1.82 (*m*); 2.13 (*m*)	-	-	1.27 (*m*); 1.87 (*m*)
17	-	-	5.60 (*s*)	5.47 (*s*)	2.05 (*td*, 10.53; 7.16)
18	1.37 (*m*)	1.51 (*m*)	1.24 (*s*)	1.13 (*s*)	1.03 (*s*)
19	0.89 (*m*)	2.18 (*m*); 1.38 (*m*)	1.20 (*s*)	1.36 (*s*)	0.98 (*s*)
20	0.86 (*m*)	-	-	-	-
21	1.24 (*m*); 1.34 (*m*)	2.43 (*m*); 1.64 (*m*)	7.41 (*s*)	7.41 (*s*)	1.21 (*s*)
22	1.24 (*m*); 1.41 (*m*)	1.31 (*m*); 1.70 (*m*)	6.35 (*s*)	6.36 (*s*)	1.41 (*m*); 1.68 (*m*)
23	1.06 (*s*)	1.06 (*s*)	7.40 (*d*, 1.70)	7.39 (*d*, 0.95)	2.05 (*m*); 2.17 (*m*)
24	1.03 (*s*)	1.09 (*s*)	-	-	5.17 (*t*, 7.04)
25	1.05 (*s*)	1.03 (*s*)	-	-	-
26	1.07 (*s*)	0.96 (*s*)	-	-	1.70 (*s*)
27	-	0.85 (*s*)	-	-	1.64 (*s*)
28	0.84 (*s*)	1.03 (*s*)	1.14 (*s*)	1.16 (*s*)	1.05 (*s*)
29	0.79 (*d*, 5.5)	-	1.10 (*s*)	1.14 (*s*)	1.08 (*s*)
30	0.86 (*brs*)	1.22 (*s*)	1.09 (*s*)	1.22 (*s*)	0.89 (*s*)

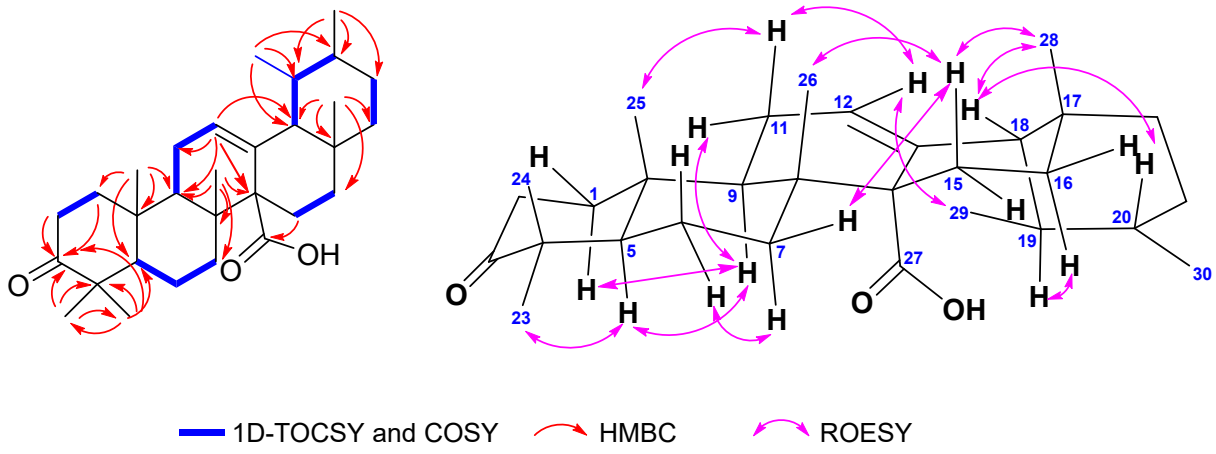


Figure 2. TOCSY-1D, HMBC, and ROESY correlation of **2**.

2.2. Antibacterial Evaluation

Preliminary antibacterial evaluation of all isolated compounds, prepared at a concentration of 1 mg/mL (equivalent to 10 µg per disk), against two Gram-positive (*E. faecalis* and *S. saprophyticus*) and two Gram-negative (*C. freundii* and *S. enterica*) bacteria showed that only **7** inhibited the growth of the tested bacteria (Table 3).

Table 3. Antibacterial activities of Compounds **1**–**7**.

Compounds	Inhibition Zone Diameter (mm)			
	Gram-Positive Bacteria		Gram-Negative Bacteria	
	E. faecalis	*S. saprophyticus*	*S. enterica*	*C. freundii*
Amoxicillin [(1)]	28	14	15	30
Chloramphenicol [(1)]	8	25	26	25
1	-	-	-	-
2	-	-	-	-
3	-	-	-	-
4	-	-	-	-
5	-	-	-	-
6	-	-	-	-
7	9	7.5	8	9
5% DMSO-MHB [(2)]	-	-	-	-

[(1)] Positive control. [(2)] Solvent, negative control.

2.3. Study of Density Functional Theory (DFT)

To further explore these reactivity parameters, Density Functional Theory (DFT) calculations on the B3LYP/6-31+g(d,p) level were conducted on compounds **1**–**7**. These results, summarized in Table 4, provide insight into important reactivity descriptors like the HOMO-LUMO energy gap, chemical hardness, and electrophilicity index. The HOMO-LUMO energy gap is a vital factor in determining the reactivity and stability of a molecule. A smaller gap signifies higher reactivity and lower stability, while a larger gap suggests greater stability and reduced reactivity.

Table 4. Calculated molecular orbital energies and chemical reactivity descriptors.

Compound	E_{HOMO}	E_{LUMO}	IP	EA	χ	μ	η	ω	E_g
1	−6.487	−0.142	6.49	0.14	3.31	−3.31	3.17	1.73	6.34
2	−6.565	−0.736	6.56	0.74	3.65	−3.65	2.91	2.29	5.83
3	−6.174	−0.587	6.17	0.59	3.38	−3.38	2.79	2.05	5.59
4	−6.667	−1.967	6.67	1.97	4.32	−4.32	2.35	3.96	4.70
5	−6.740	−2.195	6.74	2.20	4.47	−4.47	2.27	4.39	4.54
6	−6.351	−0.756	6.35	0.76	3.55	−3.55	2.80	2.26	5.59
7	−6.331	−0.458	6.33	0.46	3.39	−3.39	2.94	1.96	5.87

Ionization potential (IP), electron affinity (EA), electronegativity (χ), chemical potential (μ), chemical hardness (η), electrophilicity (ω), HOMO-LUMO energy gap (E_g). All values are in eV units.

Our results indicate that compound **5** has the smallest HOMO-LUMO energy gap (4.54 eV), making it the most reactive and least stable molecule in the set. In contrast, Compound **1**, with the largest HOMO-LUMO energy gap (6.34 eV), is the most stable but exhibited lower reactivity. This large gap in Compound **1** limits its ability to undergo electronic transitions, which decreases its reactivity.

Other compounds, such as **2**, **3**, **6**, and **7**, exhibit intermediate values for the HOMO-LUMO gap, ranging from 5.59 to 5.87 eV, indicating moderate reactivity. The electrophilicity indices for these compounds fall between 1.96 and 2.29 eV, suggesting they have a moderate tendency to accept electrons. Their ionization potential and electron affinities also support this, ranging from 6.17 to 6.56 eV and 0.46 to 0.76 eV, respectively. These compounds are, therefore, characterized by a balance of stability and reactivity, making them versatile candidates for various chemical applications.

Compound **5** is characterized by high reactivity and low stability, as evidenced by its small HOMO-LUMO energy gap and high electrophilicity index (4.39 eV), along with a significant ionization potential (6.74 eV) and electron affinity (2.20 eV). Meanwhile, compound **1**, with a low electrophilicity index (1.73 eV), low ionization potential (6.49 eV), and low electron affinity (0.14 eV), is the most stable and least reactive compound.

2.4. Molecular Docking Study

PTP1B plays a role in microbial signaling pathways, including cell growth, migration, communication, and gene transcription [31,32]. Owing to these regulations, PTP1B protein is a reliable target protein for understanding the molecular inhibitory mechanisms of small-molecule compounds as antibacterial agents [32]. Moreover, compound **7** was selected because of its promising activity against *E. faecalis* compared to the isolated compounds (**1**–**6**) and chloramphenicol as a control (Table 3). Therefore, compounds **7** and chloramphenicol were modeled to investigate their interactions at the molecular level.

Cluster spheres were built along the targeted protein surface to determine the possibility of pocket site coordination. The accurate coordinates were then selected based on the native ligand coordinates as a reference with a radius of 10 Å. Through the coordination, the grid box was prepared to obtain the PTP1B pocket site (Figure 3). The superposition shows a root-mean-square deviation (RMSD) of 1.01 Å (Figure 4). This finding indicates that the parameters utilized in the redocking step can be used as coordinates on the PTP1B pocket site. This validation also confirmed several amino acids that act as catalytic sites (CS), namely H213, C214, S215, A216, G217, I218, G219, and R220 [32]. As expected, the interaction between the modeled small molecules and the CS region can provide information about the inhibitory mechanism of the active compound's antibacterial activity.

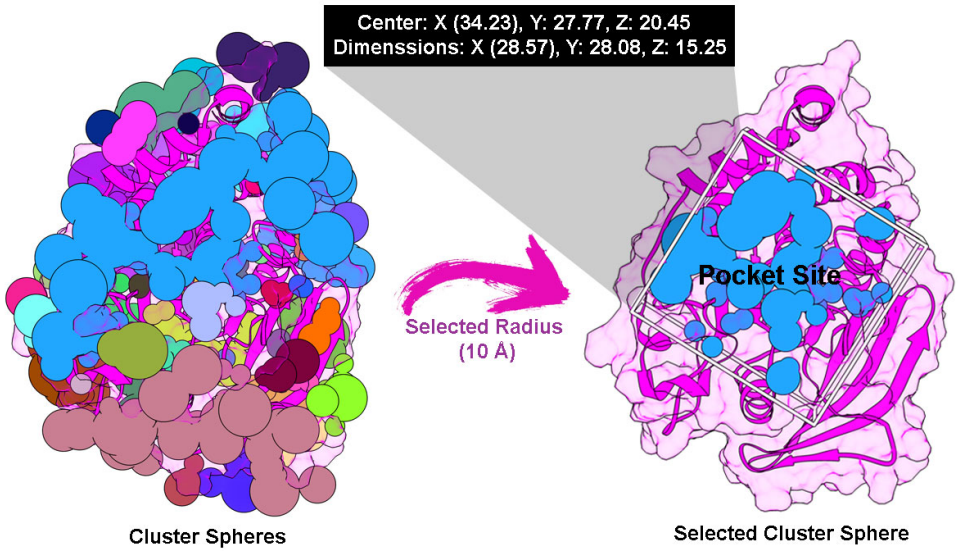


Figure 3. Grid-box preparation: The cluster spheres represent the possibility of a binding site. The selected cluster sphere represents the PTP1B pocket site (blue). The box parameters, such as the center and dimensions, were determined by coordinating the selected spheres.

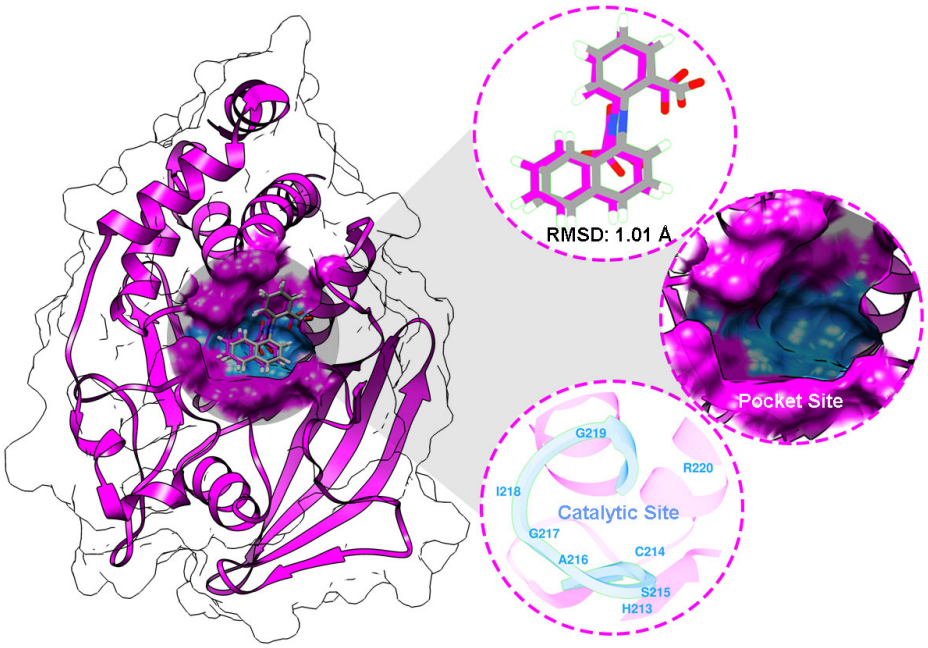


Figure 4. Redocking step: Protein Tyrosine Phosphatase 1B (PTP1B) crystal structure as a targeted protein. Superposition of the native ligand between the crystal (purple) and pose (grey). PTP1B pocket and catalytic sites (blue).

Docking results revealed that the modeled molecules were well-occupied on the PTP1B binding site (Figure 5). The binding conformation shows that the grid score (GS) forms a stable interaction for chloramphenicol and the compound **7** complex, with the scores of −47.81 and −57.16 kcal/mol, respectively.

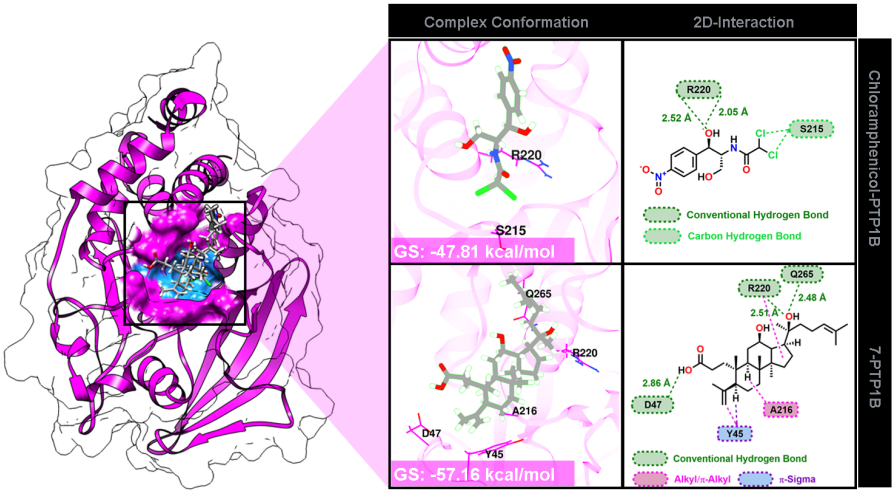


Figure 5. The ligand-PTP1B interaction was presented by complex conformation and 2D interaction.

3. Discussion

In this study, we report the isolation of terpenoids from *S. koetjape*. Among the isolated compounds, only **7** exhibited antibacterial activity. The inhibition zone of **7** against the Gram-positive bacterium *E. faecalis* was slightly larger than that of the positive control (chloramphenicol). Compounds **6** and **7** possess similar skeletons, except for the ring A opening and the existence of a carboxylic acid group in **7**. However, **6** showed no antibacterial activity, suggesting that the ring A seco-triterpenoid with a free carboxylic group found in **7** might be an important factor for antibacterial activity. In a previous study, olenane-type and seco-olenanane pentacyclic triterpenes were tested for antibacterial activities. Among the tested compounds, a seco-oleanane derivative, Koetjapic acid, exhibited the most potent antibacterial activity against *S. aureus* and *P. aeruginosa* [33]. Furthermore, 3,4-seco triterpenoids with a free carboxylic (C-3) isolated from *Dysoxylum hainanense* also showed significant antibacterial activities against some Gram-positive bacteria [34].

The DFT analysis provided valuable information regarding the electronic profiles and reactivities of all compounds. This analysis highlights the potential for tuning the reactivity of molecules by adjusting key electronic properties, such as the HOMO-LUMO energy gap and electrophilicity index, allowing for the design of molecules with specific reactivity profiles for diverse chemical applications.

Docking studies suggested that the favorable binding affinity of compound **7** was stronger than that of chloramphenicol as a control. This finding is related to the in vitro test results shown in Table 3. As mentioned previously, the van der Waals (E_{vdW}) and electrostatic (E_{ele}) energies contribute to the GS value [35]. The energy contributions of each complex were as follows: chloramphenicol-PTP1B (E_{vdW}: −46.56 kcal/mol and E_{ele}: −1.25 kcal/mol) and **7**-PTP1B (E_{vdW}: −55.70 kcal/mol and E_{ele}: −1.45 kcal/mol). As described, E_{ele} contributes significantly to the GS value. Moreover, several interactions with amino acids were confirmed through the PTP1B pocket site (Figure 5). Several molecular interactions were included in each complex, such as conventional hydrogen bonds, alkyl/π-alkyl, π-sigma, and carbon–hydrogen bonds. Interestingly, compound **7** interacted with CS amino acids, including R220 (hydrogen bond) and A216 (π-alkyl). It is known that interaction with amino acid residues around the CS region can block PTP1B enzymatic regulation of microbial growth.

4. Materials and Methods

4.1. General

Optical rotations were determined using an Autopol IV polarimeter (Rudolph Research Analytical, Hackettstown, NJ, USA). ^{1}H-NMR and ^{13}C-NMR were recorded with a spectrometer of the Agilent DD2 system (Agilent Technologies, Santa Clara, CA, USA) operating at 500 and 125 MHz, respectively. Mass spectra were measured with Waters LCT Premier XE ESI-TOF-MS (Waters Corporation, Milford, MA, USA). Silica gels (Merck, Darmstadt, Germany) were used for all chromatographic separations. Vacuum Liquid Chromatography (VLC), Centrifugal Planar Chromatography (CPC), and Column Chromatography (CC) were carried out on Merck silica gel G60 254 art. 7731, 7749, and 7733, respectively. Thin-layer chromatography (TLC) analysis was performed using precoated silica gel 60 GF254 plates (0.25 mm thickness; Merck, Darmstadt, Germany). Spots on TLC were detected by UV irradiation and sprayed with $CeSO_4$ solution followed by heating. Solvents used for extraction, fractionation, and purification (MeOH, EtOAc, dichloromethane, and *n*-hexane) were of technical grades, which were distilled before use, while $CHCl_3$ and diisopropyl ether were of a pro analysis grade. *Enterococcus faecalis* (ATCC 29212), *Staphylococcus saprophyticus* (ATCC 19701), *Citrobacter freundii* (ATCC 13316), and *Salmonella enterica* (ATCC 14028) were obtained from the Microbiology Laboratory, Faculty of Medicine, Universitas Jenderal Soedirman, Purwokerto, Indonesia.

4.2. Plant Materials

The tree barks of *S. koetjape* were collected from Pandeglang, Banten Province, Indonesia, in August 2013. Plant identification was performed at the Herbarium Bandungense, Institut Teknologi Bandung (voucher specimen number 11254).

4.3. Extraction and Isolation

The dried tree barks of *S. koetjape* powders (1.0 kg) were macerated with MeOH (2 × 10 L, overnight) at room temperature to obtain 61.0 g of dried MeOH extract. Half of the extract (30.0 g) was fractionated into 17 fractions (A–Q) by VLC (silica gel, gradient eluent: *n*-hexane—EtOAc 15% to 70%, then EtOAc and MeOH). Fractions D–E (2.7 g) were separated by VLC eluted with *n*-hexane—EtOAc 15% to 20%, then EtOAc and MeOH generated 14 fractions (DE1–DE14). Fraction DE2 (503.8 mg) was further purified by CPC (eluent: *n*-hexane—$CHCl_3$ 10% to 100%) to yield **1** (12.0 mg). Fraction DE14, which was found to be a white solid and showed a single spot on TLC, was filtered to obtain **3** (15.3 mg). Fraction F (1.46 g) was fractionated using VLC (silica gel, gradient eluent: *n*-hexane—EtOAc 5% to 20%, then EtOAc and MeOH) to give 14 fractions (F1–F14). Fractions F11–12 (190.0 mg) were separated by CPC (eluent: *n*-hexane—EtOAc 5% to 20%) then successfully purified using the same method (eluent: *n*-hexane—diisopropyl ether 40%), which afforded **2** (18.5 mg). Fraction L (884.6 mg) was fractionated by CPC using gradient eluent *n*-hexane—EtOAc 20% to 50%, yielding 34 fractions. Fractions L4–L9 (191.9 mg) were separated using a similar method (eluent: *n*-hexane–dichloromethane–EtOAc 7:2:1) afforded **6** (8.5 mg). The fraction then further purified by CC (eluent: $CHCl_3$ 100%) gave **4** (8.5 mg). A white solid appeared on fraction N (1.32 g), which showed a minor spot on TLC. The solid then filtered and washed with *n*-hexane to give **5** (27.5 mg). In our previous work, we reported the isolation of **7** from the polar fraction P (1.87 g). A solid (390.0 mg) appeared from the fraction, which showed a minor impurity on the TLC analysis, and which was purified by VLC (eluent: *n*-hexane—EtOAc 20%) to afford **7** (60.0 mg) [24].

β-caryophyllene oxide (**1**)—yellowish oil, $[\alpha]^{25}_{D}$ −40.0 (c 0.1; $CHCl_3$) ^{1}H-NMR ($CDCl_3$, 500 MHz), δ_H (ppm) 1.76 (1H, t; 9.92 Hz, H-1); 1.43 (1H, m, H-2); 1.65 (1H, m, H-2); 0.97 (1H, m, H-3); 2.09 (1H, dt; 13.15 Hz; 4.19 Hz, H-3); 2.88 (1H, dd; 10.6 Hz; 4.3 Hz, H-5); 2.34 (1H,

ddd, 12.70 Hz; 8.07 Hz; 4.46 Hz, H-6); 1.25 (1H, d; 3.58 Hz, H-6); 1.33 (2H, m, H-7); 2.61 (1H, q; 9.5 Hz, H-9); 1.65 (2H, m, H-10); 1.20 (3H, s, H-12); 4.86 (1H, s, H-13); 4.97 (1H, s, H-13); 0.98 (3H, s, H-14); 1.01 (3H, s, H-15). ^{13}C-NMR ($CDCl_3$, 125 MHz), δ_C (ppm) 50.8 (C-1); 27.2 (C-2); 39.2 (C-3); 59.8 (C-4); 63.8 (C-5); 29.8 (C-6); 30.2 (C-7); 151.8 (C-8); 48.7 (C-9); 39.8 (C-10); 34.0 (C-11); 17.0 (C-12); 112.8 (C-13); 29.9 (C-14); 21.6 (C-15). HRESITOF-MS: $[M+H]^+$ ion m/z 221.1908 (calcd. $[M+H]^+$ ion for $C_{15}H_{24}O$: m/z 221.1905; Δ 1.4 ppm). The NMR and mass spectra of compound **1** are available in the supplementary file (Figures S1–S5).

(18β,19αH)-3-oxo-urs-12-en-27α-oic acid (**2**)—white powders, $[\alpha]^{23}_D$ +142.0 (c 0.1; $CHCl_3$). ^{13}C-NMR (in $CDCl_3$) see Table 2; ^{1}H-NMR see Table 1. HRESITOF-MS: $[M-H]^-$ ion m/z 453.3367 (calcd. $[M-H]^-$ ion for $C_{30}H_{46}O_3$: m/z 453.3369; Δ 0.4 ppm). The NMR and mass spectra of compound **2** are available in the supplementary file (Figures S6–S12).

Bryononic acid (**3**)—white powders, $[\alpha]^{23}_D$ +36.0 (c 0.1; $CHCl_3$). ^{13}C-NMR (in $CDCl_3$) see Table 2; ^{1}H-NMR see Table 1. HRESITOF-MS: $[M-H]^-$ ion m/z 453.3356 (calcd. $[M-H]^-$ ion for $C_{30}H_{46}O_3$: m/z 453.3369; Δ 2.9 ppm). The NMR and mass spectra of compound **3** are available in the supplementary file (Figures S13–S18).

7-deacetyl gedunin (**4**)—white powders, $[\alpha]^{23}_D$ +46.0 (c 0.1; $CHCl_3$). ^{13}C-NMR (in $CDCl_3$) see Table 2; ^{1}H-NMR see Table 1. HRESITOF-MS: $[M+H]^+$ ion m/z 441.2285 (calcd. $[M+H]^+$ ion for $C_{26}H_{32}O_6$: m/z 441.2277; Δ 1.8 ppm). The NMR and mass spectra of compound **4** are available in the supplementary file (Figures S19–S23).

7-deacetyl-7-oxogedunin (**5**)—white powders, $[\alpha]^{23}_D$ −62.0 (c 0.1; $CHCl_3$). ^{13}C-NMR (in $CDCl_3$) see Table 2; ^{1}H-NMR see Table 1. HRESITOF-MS: $[M+H]^+$ ion m/z 439.2123 (calcd. $[M+H]^+$ ion for $C_{26}H_{30}O_6$: m/z 439.2121; Δ 0.5 ppm). The NMR and mass spectra of compound **5** are available in the supplementary file (Figures S24–S28).

12,20-dihydroxydammar-24-en-3-one (**6**)—white powders, $[\alpha]^{23}_D$ +24.0 (c 0.1; $CHCl_3$). ^{13}C-NMR (in $CDCl_3$) see Table 2; ^{1}H-NMR see Table 1. HRESITOF-MS: $[M+H]^+$ ion m/z 459.3835 (calcd. $[M+H]^+$ ion for $C_{30}H_{50}O_3$: m/z 459.3838; Δ 0.7 ppm). The NMR and mass spectra of compound **6** are available in the supplementary file (Figures S29–S33).

4.4. In Vitro Antibacterial Activity

The antibacterial activity of isolated compounds was evaluated using the disk diffusion method as a preliminary screening assay, as described in [36], against two Gram-positive (*E. faecalis* and *S. saprophyticus*) and two Gram-negative (*C. freundii* and *S. enterica*) bacteria.

4.5. DFT Calculation

Density Functional Theory (DFT) calculations were performed to achieve geometric optimization, and frequency analysis was conducted for isolated compounds (**1**–**7**) using the B3LYP/6-31+G(d,p) [37,38] level of theory with the Gaussian 16 software package [39]. The resulting data were visualized using GaussView 6.0.16 software [40]. The DFT results were used to analyze the quantum chemical characteristics, including the E_{HOMO}, E_{LUMO}, chemical hardness, softness, electronegativity, and chemical potential. Additionally, Koopman's theorem [41] was applied to calculate the numerical values of several parameters, such as the ionization potential and electron affinity.

4.6. Molecular Docking

The crystal structure of Protein Tyrosine Phosphatase 1B (PTP1B) was obtained from the Protein Data Bank with PDB ID: 1NO6 (https://www.rcsb.org/structure/1no6, accessed on 4 April 2025) as the target protein [42]. The protein was protonated at pH 7.0 using the H++ web server (http://newbiophysics.cs.vt.edu/H++/, accessed on 4 April 2025). Meanwhile, 2-[(carboxycarbonyl)(1-naphthyl)amino]benzoic acid, a native ligand, was extracted, and its coordinates were used as a reference to identify the PTP1B pocket site. The modeled small molecules were prepared using the antechamber with the General

Amber Force Field (GAFF) [43] to calculate the restrained charge, bonded, and nonbonded. Molecular docking was performed using the Dock6 package. The redocking step determined the pocket site according to the native ligand coordinates. Several crucial parameters were applied, including grid spacing (0.3 Å), center (X: 34.23, Y: 27.77, Z: 20.45), and dimensions (X: 28.57, Y: 28.08, and Z: 15.25 Å). It should be noted that an RMSD $\leq$ 2.0 Å is acceptable for redocking validation [44]. The validated parameters from the redocking step were applied to dock modeled small molecules to the PTP1B pocket site. The anchor-and-grow algorithm [45] was utilized for the ligand–protein energy interaction through the grid score (GS). In detail, the van der Waals (E_{vdW}) and electrostatic (E_{ele}) energies are described as the energy contributions in gas terms [44,45].

5. Conclusions

An ursane-type pentacyclic triterpene, (18β,19αH)-3-oxo-urs-12-en-27α-oic acid (**2**), has been isolated as a new natural compound from the tree bark of *S. koetjape*. Six known compounds, namely β-caryophyllene oxide (**1**), bryononic acid (**3**), 7-deacetylgedunin (**4**), 7-deacetyl-7-oxogedunin (**5**), 12,20-dihydroxydammar-24-en-3-one (**6**), and 12-hydroxydammarenolic acid (**7**), were also isolated from the MeOH extract of the tree bark. All compounds were assayed against *E. faecalis*, *S. saprophyticus*, *C. freundii*, and *S. enterica* bacteria. In addition, DFT analysis was performed to calculate the electronic properties of all the compounds. Of the compounds, only **7** was active against the four tested bacteria. The molecular interaction of **7** was examined using molecular docking, which revealed that the potent compound interacted well with the catalytic sites of the enzyme, which contributes to microbial growth.

Supplementary Materials: The following supporting information can be downloaded at https://www.mdpi.com/article/10.3390/ijms262110389/s1.

Author Contributions: Conceptualization, A.D. and E.H.; Methodology, H.K., F.M. and M.I.A.; Software, F.M., T.K. and M.I.A.; Validation, A.D., E.H., F.M., T.K. and M.I.A.; Formal Analysis, H.K., F.M., T.K. and M.I.A.; Investigation, H.K., F.M., T.K. and M.I.A.; Resources, A.D., E.H., F.M., T.K. and M.I.A.; Data Curation, A.D., E.H., F.M. and M.I.A.; Writing—Original Draft Preparation, H.K., F.M. and M.I.A.; Writing—Review and Editing, A.D., E.H., H.K., F.M., T.K. and M.I.A.; Visualization, H.K., F.M. and M.I.A.; Supervision, A.D. and E.H.; Project Administration, A.D. and E.H.; Funding Acquisition, A.D. and E.H. All authors have read and agreed to the published version of the manuscript.

Funding: This research received no external funding.

Institutional Review Board Statement: Not applicable.

Informed Consent Statement: Not applicable.

Data Availability Statement: The original contributions presented in this study are included in the article/Supplementary Materials. Further inquiries can be directed to the corresponding authors.

Acknowledgments: This research is funded by the Indonesian Endowment Fund for Education (LPDP) on behalf of the Indonesian Ministry of Higher Education, Science and Technology and managed under the EQUITY Program (Contract No. 4298/B3/DT.03.08/2025). The authors are grateful to the Unggulan Scholarship, the Ministry of Education and Culture of Indonesia, for the master's degree fellowship awarded to H.K. The authors also thank Basic Science Center A and the Directorate for Multidisciplinary Science and Technology Applications (DIPTM), Institut Teknologi Bandung, for providing excellent facilities and support during the research. F.M. and T.K. sincerely appreciate the computational resources provided by the Faculty of Advanced Technology and Multidiscipline at Universitas Airlangga, in addition to the high-performance computing services and facilities offered by the NSTDA Supercomputer Center (ThaiSC).

Conflicts of Interest: The authors declare that there are no conflicts of interest.

References

1. Arora, G.; Sajid, A.; Kalia, V.C. *Drug Resistance in Bacteria, Fungi, Malaria, and Cancer*; Springer: Cham, Switzerland, 2017; pp. 1–629. [CrossRef]
2. WHO. *WHO Bacterial Priority Pathogens List, 2024*; WHO: Geneva, Switzerland, 2024.
3. Chellat, M.F.; Raguž, L.; Riedl, R. Targeting Antibiotic Resistance. *Angew. Chem. Int. Ed.* **2016**, *55*, 6600–6626. [CrossRef]
4. Moloney, M.G. Natural Products as a Source for Novel Antibiotics. *Trends Pharmacol. Sci.* **2016**, *37*, 689–701. [CrossRef]
5. Newman, D.J.; Cragg, G.M. Natural Products as Sources of New Drugs over the Nearly Four Decades from 01/1981 to 09/2019. *J. Nat. Prod.* **2020**, *83*, 770–803. [CrossRef]
6. Mahizan, N.A.; Yang, S.K.; Moo, C.L.; Song, A.A.L.; Chong, C.M.; Chong, C.W.; Abushelaibi, A.; Erin Lim, S.H.; Lai, K.S. Terpene Derivatives as a Potential Agent against Antimicrobial Resistance (AMR) Pathogens. *Molecules* **2019**, *24*, 2631. [CrossRef] [PubMed]
7. Wang, C.M.; Chen, H.T.; Wu, Z.Y.; Jhan, Y.L.; Shyu, C.L.; Chou, C.H. Antibacterial and Synergistic Activity of Pentacyclic Triterpenoids Isolated from Alstonia Scholaris. *Molecules* **2016**, *21*, 139. [CrossRef] [PubMed]
8. Kazakova, O.; Tret'yakova, E.; Baev, D. Evaluation of A-Azepano-Triterpenoids and Related Derivatives as Antimicrobial and Antiviral Agents. *J. Antibiot.* **2021**, *74*, 559–573. [CrossRef]
9. Kazakova, O.B.; Brunel, J.M.; Khusnutdinova, E.F.; Negrel, S.; Giniyatullina, G.V.; Lopatina, T.V.; Petrova, A.V. A-Ring-Modified Triterpenoids and Their Spermidine–Aldimines with Strong Antibacterial Activity. *Molbank* **2019**, *2019*, M1078. [CrossRef]
10. Bailly, C. The Health Benefits of Santol Fruits and Bioactive Products Isolated from Sandoricum Koetjape Merr.: A Scoping Review. *J. Food Biochem.* **2022**, *46*, e14152. [CrossRef]
11. Bumi, M.B.; Heliawaty, L.; Hermawati, E.; Syah, Y.M. Four Limonoids from the Seeds Extract of Sandoricum Koetjape. *J. Nat. Med.* **2019**, *73*, 641–647. [CrossRef]
12. Efdi, M.; Ninomiya, M.; Suryani, E.; Tanaka, K.; Ibrahim, S.; Watanabe, K.; Koketsu, M. Sentulic Acid: A Cytotoxic Ring A-Seco Triterpenoid from Sandoricum Koetjape Merr. *Bioorganic Med. Chem. Lett.* **2012**, *22*, 4242–4245. [CrossRef] [PubMed]
13. Rachmadhaningtiyas, D.A.; Heliawati, L.; Hermawati, E.; Syah, Y.M. A Cipadesin Limonoid and a Tirucallane Triterpene from the Fruit of Sandoricum Koetjape and Their Inhibitory Properties against Receptor Tyrosine Kinases. *Nat. Prod. Sci.* **2021**, *27*, 134–139. [CrossRef]
14. Kaneda, N.; Pezzuto, J.M.; Kinghorn, D.; Farnsworth, N.R.; Santisuk, T.; Tuchinda, P.; Udchachon, J.; Reutrakul, V. Plant Anticancer Agents, l. Cytotoxic Triterpenes from Sandoricum Koetjape Stems. *J. Nat. Prod.* **1992**, *55*, 654–659. [CrossRef]
15. Ismail, I.S.; Ito, H.; Hatano, T.; Taniguchi, S.; Yoshida, T. Modified Limonoids from the Leaves of Sandoricum Koetjape. *Phytochemistry* **2003**, *64*, 1345–1349. [CrossRef]
16. Ismail, I.S.; Ito, H.; Hatano, T.; Taniguchi, S.; Yoshida, T. Two New Analogues of Trijugin-Type Limonoids from the Leaves of Sandoricum Koetjape. *Chem. Pharm. Bull.* **2004**, *52*, 1145–1147. [CrossRef]
17. Kosela, S.; Yulizar, Y.; Chairul, C.; Tori, M.; Asakawa, Y. Secomultiflorane-Type Triterpenoid Acids from Stem Bark of Sandoricum Koetjape. *Phytochemistry* **1995**, *38*, 691–694. [CrossRef]
18. Nagakura, Y.; Nugroho, A.E.; Hirasawa, Y.; Hosoya, T.; Rahman, A.; Kusumawati, I.; Zaini, N.C.; Morita, H. Sanjecumins A and B: New Limonoids from Sandoricum Koetjape. *J. Nat. Med.* **2013**, *67*, 381–385. [CrossRef]
19. Pancharoen, O.; Pipatanapatikarn, A.; Charles Taylor, W.; Bansiddhi, J. Two New Limonoids from the Leaves of Sandoricum Koetjape. *Nat. Prod. Res.* **2009**, *23*, 10–16. [CrossRef]
20. Powell, R.G.; Mikolajczak, K.L.; Zilkowski, B.W. Limonoid Antifeedants from Seed of Sandoricum Koetjape. *J. Nat. Prod.* **1991**, *54*, 241–246. [CrossRef]
21. Tanaka, T.; Koyano, T.; Kowithayakorn, T.; Fujimoto, H.; Okuyama, E.; Hayashi, M.; Komiyama, K.; Ishibashi, M. New Multiflorane-Type Triterpenoid Acids from Sandoricum Indicum. *J. Nat. Prod.* **2001**, *64*, 1243–1245. [CrossRef] [PubMed]
22. Saptanti, K.; Heliawati, L.; Hermawati, E.; Syah, Y.M. Pentacyclic Triterpenes from the Leaves Extract of Sandoricum Koetjape. *J. Nat. Med.* **2022**, *76*, 842–848. [CrossRef] [PubMed]
23. Hang, T.-X.-H.; Jarupinthusophon, S.; Hairani, R.; Nguyen, V.-K.; Chavasiri, W. Cycloartane-Type Triterpenoids from the Leaves of Sandoricum Koetjape and Their Efficacy on α-Glucosidase Inhibition Activity. *J. Nat. Med.* **2024**, *78*, 655–663. [CrossRef]
24. Heliawati, L.; Khatimah, H.; Hermawati, E.; Syah, Y.M. Four Dammarane Triterpenes and Their Inhibitory Properties against Eight Receptor Tyrosine Kinases. *Nat. Prod. Sci.* **2020**, *26*, 345–350. [CrossRef]
25. Nsiama, T.K.; Okamura, H.; Hamada, T.; Morimoto, Y.; Doe, M.; Iwagawa, T.; Nakatani, M. Rings D-Seco and B,D-Seco Tetranortriterpenoids from Root Bark of Entandrophragma Angolense. *Phytochemistry* **2011**, *72*, 1854–1858. [CrossRef]
26. Nagatomo, A.; Ninomiya, K.; Marumoto, S.; Sakai, C.; Watanabe, S.; Ishikawa, W.; Manse, Y.; Kikuchi, T.; Yamada, T.; Tanaka, R.; et al. A Gedunin-Type Limonoid, 7-Deacetoxy-7-Oxogedunin, from Andiroba (Carapa Guianensis Aublet) Reduced Intracellular Triglyceride Content and Enhanced Autophagy in HepG2 Cells. *Int. J. Mol. Sci.* **2022**, *23*, 13141. [CrossRef]
27. Chen, J.J.; Fei, D.Q.; Chen, S.G.; Gao, K. Antimicrobial Triterpenoids from Vladimiria Muliensis. *J. Nat. Prod.* **2008**, *71*, 547–550. [CrossRef]

28. Cai, X.F.; Park, B.Y.; Ahn, K.S.; Kwon, O.K.; Lee, H.K.; Oh, S.R. Cytotoxic Triterpenoids from the Rhizomes of Astilbe Chinensis. *J. Nat. Prod.* **2009**, *72*, 1241–1244. [CrossRef]
29. Razdan, T.K.; Kachroo, V.; Harkar, S.; Koul, G.L. Plectranthoic Acid A & B, Two New Triterpenoids from Plectranthus Rugosus. *Tetrahedron* **1982**, *38*, 991–992. [CrossRef]
30. Wu, L.; Liu, J.; Chen, K.; Zhang, L.; Li, Y. Triterpenoids from the Roots of Sanguisorba Officinalis and Their Nrf2 Stimulation Activity. *Phytochemistry* **2023**, *214*, 113803. [CrossRef] [PubMed]
31. Hale, A.J.; ter Steege, E.; den Hertog, J. Recent Advances in Understanding the Role of Protein-Tyrosine Phosphatases in Development and Disease. *Dev. Biol.* **2017**, *428*, 283–292. [CrossRef] [PubMed]
32. Alfarisi, S.; Santoso, M.; Kristanti, A.N.; Siswanto, I.; Puspaningsih, N.N.T. Synthesis, Antimicrobial Study, and Molecular Docking Simulation of 3,4-Dimethoxy-β-Nitrostyrene Derivatives as Candidate Ptp1b Inhibitor. *Sci. Pharm.* **2020**, *88*, 37. [CrossRef]
33. Muhammad, I.; El Sayed, K.A.; Mossa, J.S.; Al-Said, M.S.; El-Feraly, F.S.; Clark, A.M.; Hufford, C.D.; Oh, S.; Mayer, A.M.S. Bioactive 12-Oleanene Triterpene and Secotriterpene Acids from Maytenus Undata. *J. Nat. Prod.* **2000**, *63*, 605–610. [CrossRef] [PubMed]
34. He, X.F.; Wang, X.N.; Yin, S.; Dong, L.; Yue, J.M. Ring A-Seco Triterpenoids with Antibacterial Activity from Dysoxylum Hainanense. *Bioorganic Med. Chem. Lett.* **2011**, *21*, 125–129. [CrossRef] [PubMed]
35. Balius, T.E.; Tan, Y.S.; Chakrabarti, M. DOCK 6: Incorporating Hierarchical Traversal through Precomputed Ligand Conformations to Enable Large-Scale Docking. *J. Comput. Chem.* **2024**, *45*, 47–63. [CrossRef]
36. Klančnik, A.; Piskernik, S.; Jeršek, B.; Možina, S.S. Evaluation of Diffusion and Dilution Methods to Determine the Antibacterial Activity of Plant Extracts. *J. Microbiol. Methods* **2010**, *81*, 121–126. [CrossRef] [PubMed]
37. Le, T.K.D.; Ene, F.; Duong, T.H.; Mulya, F.; Chavasiri, W. Insights into the Inhibitory Activity and Mechanism of Natural Compounds from Rhinacanthus Nasutus on α-Glucosidase through Kinetic, Molecular Docking, and Molecular Dynamics Studies. *J. Mol. Struct.* **2025**, *1322*, 140527. [CrossRef]
38. Kaennakam, S.; Sukandar, E.R.; Phasuthan, P.; Yahuafai, J.; Onsrisawat, P.; Mulya, F.; Parasuk, V.; Phuwapraisirisan, P.; Tip-pyang, S. Garcowacinols A-J, Cytotoxic Polyprenylated Benzoylphloroglucinol Derivatives from the Twigs of Garcinia Cowa. *Phytochemistry* **2023**, *209*, 113622. [CrossRef]
39. Frisch, M.J.; Trucks, G.W.; Schlegel, H.B.; Scuseria, G.E.; Robb, M.A.; Cheeseman, J.R.; Scalmani, G.; Barone, V.; Petersson, G.A.; Nakatsuji, H.; et al. *Gaussian 16 Rev. C.01*; Gaussian Inc.: Wallingford, CT, USA, 2016.
40. Dennington, R.; Keith, T.A.; Millam, J.M. *GaussView*, version 6; Semichem Inc.: Shawnee Mission, KS, USA, 2016.
41. Tsuneda, T.; Song, J.W.; Suzuki, S.; Hirao, K. On Koopmans' Theorem in Density Functional Theory. *J. Chem. Phys.* **2010**, *133*, 174101. [CrossRef]
42. Szczepankiewicz, B.G.; Liu, G.; Hajduk, P.J.; Abad-Zapatero, C.; Pei, Z.; Xin, Z.; Lubben, T.H.; Trevillyan, J.M.; Stashko, M.A.; Ballaron, S.J.; et al. Discovery of a Potent, Selective Protein Tyrosine Phosphatase 1B Inhibitor Using a Linked-Fragment Strategy. *J. Am. Chem. Soc.* **2003**, *125*, 4087–4096. [CrossRef]
43. Wang, J.; Wolf, R.M.; Caldwell, J.W.; Kollman, P.A.; Case, D.A. Development and Testing of a General Amber Force Field. *J. Comput. Chem.* **2004**, *56531*, 1157–1174. [CrossRef]
44. Brozell, S.R.; Mukherjee, S.; Balius, T.E.; Roe, D.R.; Case, D.A.; Rizzo, R.C. Evaluation of DOCK 6 as a Pose Generation and Database Enrichment Tool. *J. Comput. Aided Mol. Des.* **2012**, *26*, 749–773. [CrossRef]
45. Allen, W.J.; Balius, T.E.; Mukherjee, S.; Brozell, S.R.; Moustakas, D.T.; Lang, P.T.; Case, D.A.; Kuntz, I.D.; Rizzo, R.C. DOCK 6: Impact of New Features and Current Docking Performance. *J. Comput. Chem.* **2015**, *36*, 1132–1156. [CrossRef] [PubMed]

Disclaimer/Publisher's Note: The statements, opinions and data contained in all publications are solely those of the individual author(s) and contributor(s) and not of MDPI and/or the editor(s). MDPI and/or the editor(s) disclaim responsibility for any injury to people or property resulting from any ideas, methods, instructions or products referred to in the content.